JOURNAL OF GEOPHYSICAL RESEARCH, VOL. 103, NO. D6, PAGES 6405-6416, MARCH 27, 1998

Rayleigh lidar measurements of the temporal frequency and vertical wavenumber spectra in the mesosphere over the Rocky Mountain region

X. Gao [1] and J. W. Meriwether

Department of Physics and Astronomy, Clemson University, Clemson, South Carolina

V. B. Wickwar, T. D. Wilkerson, and S. Collins[2]

Center of Atmospheric and Space Physics, Utah State University, Logan

Abstract. Temporal and spatial spectral analysis techniques were applied to lidar data collected over a period of 18 months above the Rocky Mountain region at an altitude range from 45 to 70 km by a Rayleigh lidar system located in Logan, Utah (41.7°N, 111.8°W). Examination of the averaged temporal frequency $F(\omega)$ and vertical wavenumber $F(m)$ spectra showed spectral slope values of -1.49 ± 0.03 and -2.3 ± 0.1, respectively. The observed slope for the overall averaged $F(m)$ spectrum is considerably more positive than the value of -3 predicted by the linear instability theory but close to the value of ~-2 that is predicted by the scale independent diffusive filtering theory using the measured $F(\omega)$ slope parameter. However, examination of the monthly averaged $F(m)$ spectra for the transition from winter to summer showed the spectra became flatter suggesting that Doppler shift effects caused by the seasonal change in the magnitude and direction of the background wind field are significant. The characteristic vertical wavelength λ_* was found to be ~12 km for the altitude region of 45-70 km. Comparison of this value with the characteristic wavelengths from other lidar observations at lower and higher altitude ranges showed an overall increase of λ_* with height. The observed enhancement of the $F(m)$ spectral magnitude in winter is believed to be caused in part by the low-frequency wave activity observed in the temperature profiles.

1. Introduction

Numerous observations have revealed similarities in both spectral magnitudes and slopes of middle-atmosphere vertical wavenumber spectra, $F(m)$, of density and wind perturbations. *VanZandt* [1982] suggested that this "universality" of $F(m)$ spectra was due to the random superposition of the gravity waves in the atmosphere, in a process also envisioned to be true for the ocean [*Garrett and Munk*, 1975]. Since then several theories have been developed with remarkable success to explain the mechanisms producing this spectral behavior.

The theories developed to explain the $F(m)$ spectrum of gravity wave oscillations that have been most frequently cited are the linear instability theory (LIT) by *Dewan and Good* [1986], the saturated-cascade theory (SCT) by *Dewan* [1994, 1997], the Doppler spreading theory (DST) by *Hines* [1991], diffusive damping theory (DDT) by *Weinstock* [1990] and the diffusive filtering theory (DFT) by *Gardner* [1994]. These theories are based on different key assumptions, and hence the mechanisms of the formation of the spectrum described by these theories are quite different. A review of these theories and their key predictions is given by *Gardner* [1996]. While several of these theories predict the same behavior for the $F(m)$ spectrum, i.e., a spectral slope of -3, the DFT predicts a spectral slope of -3 in a special case that applies only when the power index of the temporal frequency spectrum, $F(\omega)$, is equal to -2. Otherwise, it predicts the spectral slope of the $F(m)$ spectrum as a function of the power index of $F(\omega)$.

In this paper, the experimental results from the ground-based lidar observatory in the Rocky Mountains (Wickwar et al., Rayleigh lidar observations in the upper mesosphere over Utah, submitted to J. Geophys. Res., 1997)(hereinafter referred to as Wickwar et al., submitted manuscript, 1997) will be compared with predictions from the two theories represented by LIT and DFT. This mountainous region was traversed several times in the Airborne Lidar and Observations of Hawaiian Airglow and Airborne Noctilucent Cloud (ALOHA/ANLC) campaigns. These results on the spectral analysis of the ground-based measurements of atmospheric density over Utah provide new information regarding the averaged behavior of temporal frequency and vertical wavenumber spectra in the upper mesosphere region.

2. Summary of Theories Concerning the Results of Spectral Analysis of Density Fluctuations

According to *Dewan and Good* [1986], there are two different mechanisms that account for the spectral behavior of atmospheric density fluctuations, namely, the dynamic instability (Kelvin-Helmholtz instability) and convective

[1]Now at the Electro-Optic Systems Laboratory, University of Illinois, Urbana, Illinois

[2]Now at the Arecibo Observatory, Arecibo, Puerto Rico

Paper number 97JD03073.
0148-0227/98/97JD-03073$09.00

instability. When the vertical wind shear S of the horizontal wind reaches such a value that makes the Richardson number ($R_i=N^2/S^2$, N = Brunt-Vaisala frequency) become less than 0.25, turbulence is generated reducing through dissipation the wave amplitude. The limiting wave amplitude for shear instabilities is 2 N/m.

Convective instability appears when the gravity-wave induced oscillation reaches an amplitude such that the vertical gradient of the total potential temperature (the sum of the background potential temperature and the gravity-wave induced potential temperature fluctuation) is equal or less than zero, that is,

$$\frac{d\bar{\theta}}{dz}+\frac{d\theta'}{dz}\le 0. \tag{1}$$

Wave energy dissipation through turbulence will occur as the consequence of the convective instability that is generated. The limiting wave amplitude for convective instabilities is N/m. As a result of this condition, the amplitude of the $F(m)$ spectrum of the horizontal wind at wavenumber m is constrained by the threshold

$$F(m)=\alpha\frac{N^2}{m^3}, \tag{2}$$

where α is a constant ranging from ~1/2 to 1/20, depending on whether there is a monochromatic wave or a broadband of waves in a wave packet [*Wilson et al.*, 1991]. Thus the convective instability process is thought to be the dominant mechanism that contributes to the formation of the universal spectrum because its limiting amplitude is 2 times smaller than that for shear instabilities.

Gardner [1994] proposed what he called a scale-independent (SI) diffusive filtering theory. In this theory, the effective wave-induced eddy diffusivity at a given altitude is assumed to be the same for each wave regardless of its vertical wavelength and period. Both the molecular diffusivity and eddy diffusivity that are associated with the wave activity and the turbulence serve to degrade the organized bulk air movements. A key assumption in this theory is that when the vertical phase speed of the upward propagating wave ω/m is equal to or less than the effective vertical diffusion velocity mD, the wave is severely damped and completely removed from the source spectra. Thus only waves satisfying

$$mD\le\omega/m \tag{3}$$

or equivalently

$$Dm^2\le\omega \tag{4}$$

$$m\le\sqrt{\frac{\omega}{D}} \tag{5}$$

can grow in amplitude with increasing altitude free from any dissipative effects. Waves that do not satisfy the above condition are damped by diffusion and are filtered out of the source spectra. In this theory, a wave with frequency ω and vertical wavenumber m has either been filtered out and removed from the spectrum, or remains intact with the amplitude growing exponentially with height depending on whether or not (3) through (5) are satisfied.

The model source (m,ω) spectrum is generally considered not to be separable, but separability can be assumed in the range of low m and high ω. If m'_{sc} and ω'_{sc} represent the vertical size and the timescale for each of the sources, then the source spectrum is modeled as:

$$F_u^{SC}(m,\omega)=m^s\omega^{\Gamma-(s+1)/2} \tag{6}$$

for $f<\omega<\omega_{sc}$, and

$$F_u^{SC}(m,\omega)=\frac{m^s}{\omega^{p+(s+1)/2}} \tag{7}$$

for $\omega_{sc}\le\omega\le N$, where $s\ge 0$, $\Gamma\ge(s+1)/2$ and $p\ge -1/2$.

If we denote $<(u')^2>$ as the total wave variance at an altitude z where the atmosphere is characterized by an effective diffusivity D, then the joint (m,ω) spectrum can be written as

$$F_u(m,\omega)=(2\pi)^2<(u')^2>\frac{(s+1)}{m_{sc}}\left(\frac{m}{m_{sc}}\right)^s \times\frac{(\Gamma+1)(p-1)}{(p+\Gamma)\omega_{sc}}\left(\frac{\omega}{\omega_{sc}}\right)^{\Gamma-(s+1)/2} \tag{8}$$

for $f\le\omega\le\omega_{sc}$ and $m\le(\omega/D)^{1/2}$, and

$$F_u(m,\omega)=(2\pi)^2<(u')^2>\frac{(s+1)}{m_{sc}}\left(\frac{m}{m_{sc}}\right)^s \times\frac{(\Gamma+1)(p-1)}{(p+\Gamma)\omega_{sc}}\left(\frac{\omega_{sc}}{\omega}\right)^{p+(s+1)/2} \tag{9}$$

for $\omega_{sc}\le\omega\le N$ and $m\le(\omega/D)^{1/2}$, where $m_{sc}=(\omega_{sc}/D)^{1/2}$, and $<(u')^2>$ depends on the total diffusivity.

The one-dimensional ω and m spectra can be derived by integrating the source spectrum over a complete range of m and ω, respectively, that is,

$$F_u(\omega)=\frac{e^{z/H}}{2\pi}\int_0^{(\omega/D)^{1/2}}F_u^{SC}(m,\omega)dm \tag{10}$$

$$F_u(m)=\frac{e^{z/H}}{2\pi}\int_{Dm^2}^{N}F_u^{SC}(m,\omega)d\omega \tag{11}$$

According to *Gardner* [1996], at mid-latitude mesopause heights, the wave-induced diffusivity, D_{wave}, is ~330 m^2/s, the diffusivity associated with turbulence, D_{eddy}, is ~100 m^2/s, and the molecular diffusivity, D_{mol} is ~5 m^2/s. Consequently, the fact that the wave-induced diffusivity is considerably larger than the other two is the governing factor in the successful application of diffusive filtering theory. *Gardner* [1996] established the relationship between the diffusivity and the wave field shear parameter $<(\partial u/\partial z)^2>$ by using

$$\left\langle \left(\frac{\partial u}{\partial z}\right)^2 \right\rangle = \frac{N^2}{\tilde{R}_i} = \frac{1}{2\pi}\int_f^N d\omega \int_0^{m_{sc}(\omega/\omega_{sc})^{1/2}} m^2 F_u(m,\omega)dm \quad (12)$$

The vertical wavenumber spectrum and the temporal frequency spectrum now can be related to R_i through the relations

$$F_u(m) = 2\pi < (u')^2 > \frac{2(p-1)(s+1)}{(2p+s-1)}\frac{1}{m^*}\left(\frac{m}{m_*}\right)^s \qquad m < m_* \quad (13)$$

$$F_u(m) = 2\pi < (u')^2 > \frac{2(p-1)(s+1)}{(2p+s-1)}\frac{1}{m^*}\left(\frac{m_*}{m}\right)^{2p-1} \qquad m_* < m << m_b \quad (14)$$

$$F_u(\omega) = 2\pi < (u')^2 > \frac{(p-1)}{f}\left(\frac{f}{\omega}\right)^p, \qquad f < w < N \quad (15)$$

where

$$< (u')^2 >= \frac{(s+3)}{(s+1)\tilde{R}_i \ln(N/f)}\frac{N^2}{m_*^2} \quad (16)$$

for $p = 2$ and

$$< (u')^2 >= \frac{2(p-1)(s+3)}{(s+1)\tilde{R}_i (p-1)[(N/f)^{2-p} - 1]}\frac{N^2}{m_*^2} \quad (17)$$

for $p \neq 2$. In Eqs (15)-(17) we assume $\omega_{sc} = f$ so that $m_{sc} = m_*$. The predictions of the spectral behavior from the LIT and DFT theories are summarized in Table 1.

Rayleigh lidar data have been used to derive profiles of atmosphere temperature and the relative density perturbation. Spectral analysis of these atmosphere parameters can be applied to produce spectra in the vertical wavenumber and temporal frequency domains. By using the polarization relationship derived by *Hines* [1960], provided that the restriction $f << \omega << N$ holds, the relative atmospheric density perturbation profile r_a and its spectra $F_a(\omega)$ and $F_a(m)$ are related to the horizontal wind perturbation profile u' and its spectra ($F_u(\omega)$ and $F_u(m)$) through the following equations:

Table 1. Predictions of Power Law Indices

Theories	$F_u(\omega)$	$F_u(m)$
Linear instability	$\sim 1/\omega^p$	$\sim N^2/m^3$
Diffusive filtering	$\sim 1/\omega^p$	$\sim m_*^{2(p-2)} N^2/m^{2p-1}$ $p \neq 2$
		$\sim N^2/m^3, \quad p = 2$

$$|u'| = \frac{g}{N}\left|\frac{\rho_a'}{\bar{\rho}_a}\right| = \frac{g}{N}|r_a|, \quad (18)$$

$$\left\langle u'^2 \right\rangle = \left[\frac{g}{N}\right]^2 \left\langle \left[\frac{\rho_a'}{\bar{\rho}_a}\right]^2 \right\rangle = \left[\frac{g}{N}\right]^2 \left\langle r_a^2 \right\rangle, \quad (19)$$

$$F_u(\omega) = \left[\frac{g}{N}\right]^2 F_a(\omega), \quad (20)$$

$$F_u(m) = \left[\frac{g}{N}\right]^2 F_a(m). \quad (21)$$

Otherwise, if the restriction $f << \omega << N$ is not valid, it would be necessary to apply the more accurate gravity wave dispersion relation, $u' = ((1 - \omega^2/N^2)/(1 - f^2/\omega^2))^{0.5}(g/N)\, r_a$ for cases in which the radical factor departs significantly from unity.

Several lidar research groups have published results concerning the spectral analysis of temperature and density perturbation profiles. Results pertaining to the seasonal variability of both $F(m)$ and $F(\omega)$ spectral behavior for Na lidar data have been well documented by the publications from C.S. Gardner's group [*Senft and Gardner*, 1991]. Results based upon Rayleigh lidar observations have also been reported but not with such extensive detail and not as thoroughly as for the sodium lidar.

Vertical wavenumber spectra $F(m)$ using Rayleigh lidar signals backscattered from the stratosphere have been calculated by *Gardner et al.* [1989] between 35 and 50 km, by *Marsh et al.* [1991] and later by *Mitchell et al.* [1994] for the region of 30 to 45 km, and by *Senft et al.* [1993] for the height range of 20 to 45 km. *Wilson et al.* [1991] published their $F(m)$ spectra for normalized density perturbation profiles for the regions 30-45, 45-60, and 55-70 km. *Beatty et al.* [1992] have reported results for the $F(m)$ spectrum for both Rayleigh and Na lidar data at Arecibo for altitude ranges, 25-55 km, and 85-105 km as well as the results for the mesopause temporal $F(\omega)$ spectrum from the Na data. *Whiteway et al.* [1994] reported on the analysis of $F(m)$ spectrum of the potential energy using the Rayleigh lidar data collected in the Arctic region between 25 and 40 km and 40 and 55 km. *Hostetler and Gardner* [1994] published $F(m)$ and $F(k)$ spectral results from airborne Rayleigh lidar measurements, and the results for $F(\omega)$ spectra obtained by a ground-based Rayleigh lidar. The altitude range for both sets of spectra computed from the Rayleigh lidar observations was 25-40 km.

This summary illustrates that the existing published work on $F(\omega)$ and $F(m)$ spectra calculated from Rayleigh lidar data for altitudes above 50 km is sparse. The major reason for this is the relatively weak backscattering signal from altitudes >50 km caused by the lower atmosphere densities. Acquisition of the data for the calculation of the relative atmospheric density perturbation spectrum with the necessary precision for altitudes >50 km requires a more powerful Rayleigh lidar. The Utah lidar used much more power (25 W) than the Rayleigh lidars used in the citations reviewed (~4 W or less), and the Rocky Mountain location in a region of generally clear weather enabled the collection of many nights of data. Thus the Utah lidar results for the mesosphere have been applied to

study the climatology of the results from temporal frequency and vertical wavenumber spectral analysis using data collected over a 2 year period. This paper will first summarize the spectral analysis techniques used to produce $F(\omega)$ and $F(m)$ spectra and then present the results of the spectral analysis. Also included is a study of the seasonal variation of the spectral behavior which will be compared with previous results.

3. Description of Analysis Techniques

There was a total of ~200 nights of Utah observations collected in the period between August 1993 and December 1995. Because the optical components of the lidar were still being adjusted for correct alignment, the data collected from August 1993 to May 1994 were of generally good quality but with relatively weak signal returns. In the spectral analysis presented in this paper this portion of the data sets was not included. Several criteria were applied to the selection of data to insure the quality of the spectral analysis. First, all of the 2 min profiles with photocounts signal below 700 counts at 40 km altitude were excluded. Second, each nightly set of profiles was edited to remove profiles with any background abnormality (arising from instrumental noise or after-pulsing caused by too much signal in the low-altitude range bins) and to eliminate profiles with severe signal fluctuations caused by clouds drifting through the laser beam. On the basis of these criteria, for some nights only a fraction of the overall observations was used. For the $F(\omega)$ spectral analysis, an additional requirement was imposed: that is, the data series must be at least 5 hours long to ensure that enough data points were involved in the calculation of the temporal frequency spectra.

The data represented by the photocount profiles is typically 125 s long in time with 120 s consumed in signal integration and 5 s required for data transfer to hard disk storage. An average of background signals from 140 to 400 km was subtracted from these profiles. To reduce the influence of signal fluctuations caused by possible changes in sky transmittance and laser power, these profiles were normalized by the logarithm of the total sum of photocounts integrated over the profile from 40 to 140 km after removal of the background. The normalized profiles were then scaled by the square of the range for each bin to generate relative density profiles. The altitude resolution of each 2 min profile was 37.5 m, but three such samples were averaged to degrade this altitude resolution to 112.5 m before carrying out the analysis described below.

To construct the relative density perturbation profile, the unperturbed relative density model needs to be created first. This was done by two steps. The first step is to sum all of the density profiles for the night to get a nightly averaged density profile. The second step is to use a 4th-order polynomial fit to the logarithms of the nightly averaged density profile to get an unperturbed density model. *Mitchell et al.* [1990] evaluated this method for producing a model background density profile and showed it was generally reliable. The reason for using the logarithms of relative density values is to eliminate the exponential dependence of density with height so that a polynomial fitting process could be applied to the data with nearly a linear height dependence. The relative density perturbation profile, $r_a(z,t)$, was then constructed by generating a profile of the differences:

$$r_a(z,t) = \frac{\rho(z,t) - \rho_0(z,t)}{\rho_0(z,t)} \cong \log(\rho(z,t)) - \log(\rho_0(z,t)) \tag{22}$$

To increase the signal-to-noise ratio, low-pass filtering was applied to each 2 min relative density perturbation profile r_a. For the calculation of the $F(m)$ spectra, the r_a profiles were first filtered temporally at each altitude bin with a cutoff frequency selected in the truncation of Fourier coefficients to be ~0.3 times the Nyquist frequency (1/4.5 min), that is, a period of ~13 min. This value is about 2 times larger than the buoyancy period. This choice was based on a need to increase the signal-to-noise ratio, but also to include as much as possible of the high-frequency signals. In a similar way, the r_a profiles were spatially filtered before the calculation of the $F(\omega)$ spectrum. The cutoff wavenumber was set to 0.1 times the Nyquist frequency (1/225 m) for which the vertical wavelength is 2.25 km. Again, the reasoning for choosing this value for the cutoff is to increase the signal-to-noise ratio and at the same time to preserve the maximum amount of high-frequency spatial information.

Both $F(\omega)$ and $F(m)$ spectra were calculated by using a prewhitening and the postdarkening algorithm [*Dewan et al.*, 1988] that reduces the power "leakage" from the low-frequency end to high frequencies and provides more detail regarding spectral structures. A 20% cosine taper window was used in this analysis. This method was chosen after examination of several alternatives including the periodogram, the direct spectral estimation, and the parametric spectral estimation. Except for the periodogram technique, the results were similar for the other three algorithms. We found that the slope of the periodogram spectrum in the linear region was affected by power leakage from low wavenumbers. The consequence of this effect was that the power law index was considerably smaller than the results derived from the other three methods.

The spectra were smoothed by convolving the calculated spectra with a Bartlett window. If realistic atmospheric perturbations can be treated as a stationary process, the statistical error can be estimated by considering the Chi-square distribution of the magnitude of the periodogram and the variance of the inflation factor of the smoothing window. A more detailed explanation describing the effects of the windowing function on the analysis is attached as an appendix. The purpose of smoothing the spectra is to reduce the spectral variance by an order of magnitude. As explained in the appendix, the standard deviation for each point of the smoothed spectrum at any frequency is ~10% of the spectral magnitude of the spectrum at that frequency.

4. Temporal Frequency Spectra of Relative Density Perturbations

Since *VanZandt* [1982] pointed out the universality of the appearance of the mesoscale spectra, there have been few attempts to model the $F(\omega)$ spectra theoretically. The reason for this is that the Doppler effect of the background winds makes the modeling of the intrinsic spectra difficult [*Dewan*, 1991]. In practice, an experimental power law model of the frequency spectra has been widely used that takes the form, ω^{-p}, where ω is the intrinsic frequency and p is a constant ranging from ~1.67 to~2 [*Gardner*, 1993].

In this study, $F(\omega)$ spectra have been derived by using the Utah lidar data. The altitude coverage of the $F(\omega)$ spectral analysis is constrained by the signal-to-noise ratio to the range of 45-70 km. The spectra were first calculated using the maximum temporal resolution of 2 min. After subtraction of the photon noise floor, the nightly averaged and monthly av-

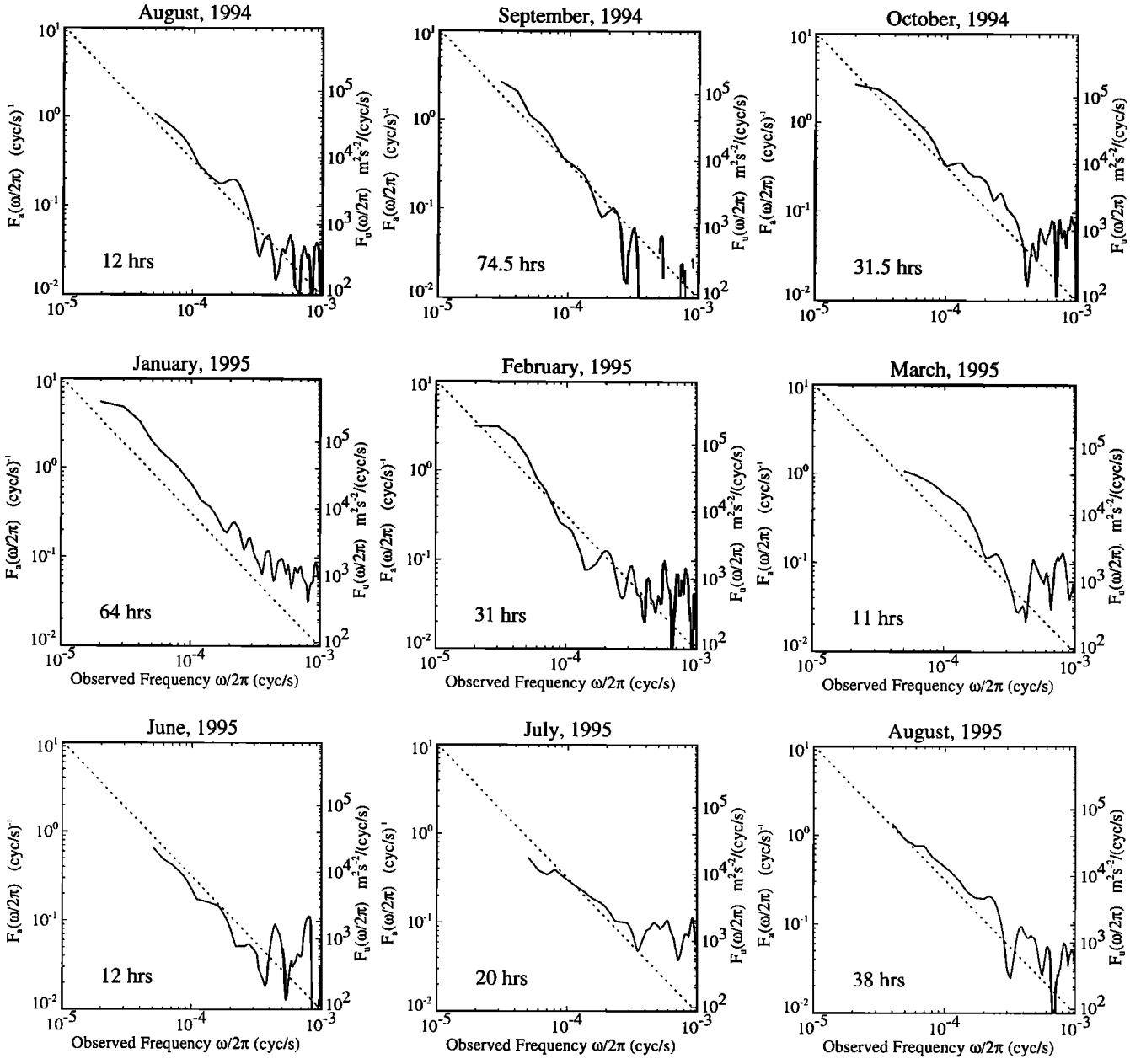

Figure 1. Monthly averaged frequency $F(\omega)$ spectra. The number of hours of observations is also indicated for each case plotted.

eraged spectra were then calculated by averaging these spectra over all observations in one night or in one month. Before this last step of averaging, the nightly-averaged spectra were interpolated so that they would have the same number of data points. The monthly averaged frequency spectra derived for the months between August 1994 and August 1995 are presented in Figure 1. The number of hours used in the averaging of each of these spectra varied from a minimum of ~12 hours in several months to a maximum of ~75 hours for September 1994. The total time of data accumulation was ~ 294 hours. The diagonal line shows for reference the slope of -1.5. Spectra of the horizontal wind perturbations can be inferred by scaling the density perturbation spectra using a factor of $(g/N)^2$ provided that the restriction $f<<\omega<<N$ is satisfied [*Mitchell et al.*, 1994].

Figure 2 shows the overall-averaged $F(\omega)$ spectrum. The spectral slope α was inferred from a linear least squares fit with an estimation of the goodness of fit based on the uncertainty of the spectral estimation at each temporal frequency. The spectral slope for the linear portion between 3×10^{-5} cycles/sec and 4×10^{-4} cycles/sec is -1.49 ± 0.03. This value is comparable to but less than the values often referred to, which range from -1.7 to -2.0 [*Gardner*, 1993].

Unfortunately, the noise floor was still high even for the monthly averaged spectra, and therefore the spectral information for time scales less than an hour was lost in the noise. However, generally, there is a linear trend that can be seen in the monthly spectra presented in Figure 1 for a log - log format. Among the 9 months of spectra plotted, 5 have spectral slopes within the range of ~ -5/3 to ~ -2 values. Inspection of

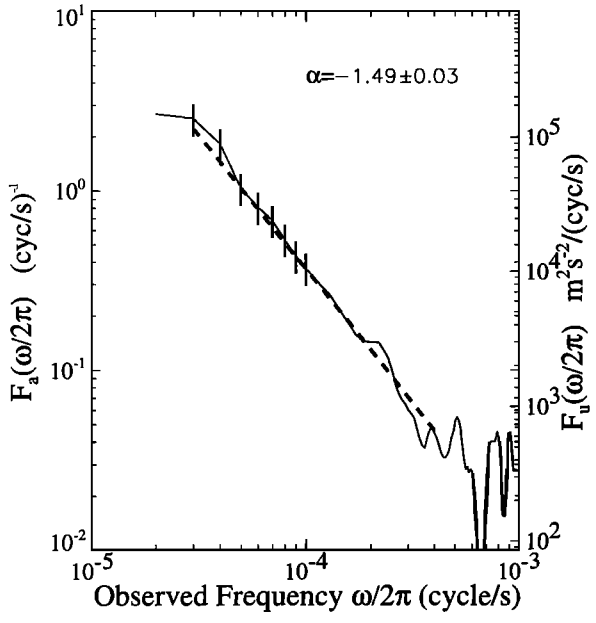

Figure 2. The overall-averaged temporal frequency spectrum. The thick dashed line is the linear least squares fit to the linear portion of the spectrum.

the monthly α values did not appear to show any overall trend for the seasonal variation of the spectral slope. As *Mitchell et al.* [1994] and *Eckermann* [1995] have noted, the Doppler shift introduced by the background wind plays an important role in the development of such trends. Since the background wind profile in the lower mesosphere region is known to reverse direction from eastward in winter to westward in summer, it is expected that there should be a seasonal trend in the parameter α if Doppler shifting effects are significant. Unfortunately, for the power-aperture product of our lidar, ~3.5 Wm^2, averaging over only few nights of observations (~10-15 hours) is not enough to reduce the statistical variability to the extent necessary to detect a trend caused by Doppler-shifting effects.

The magnitudes of the spectra at the frequency $\omega/2\pi = 10^{-4}$ (cycle/s) are plotted in Figure 3. The dotted line plotted in Figure 3 indicates the mean of the spectral magnitudes. From Figure 3 it can be seen that the magnitudes of the spectra for January and March 1995 are 1.5 times higher than the overall

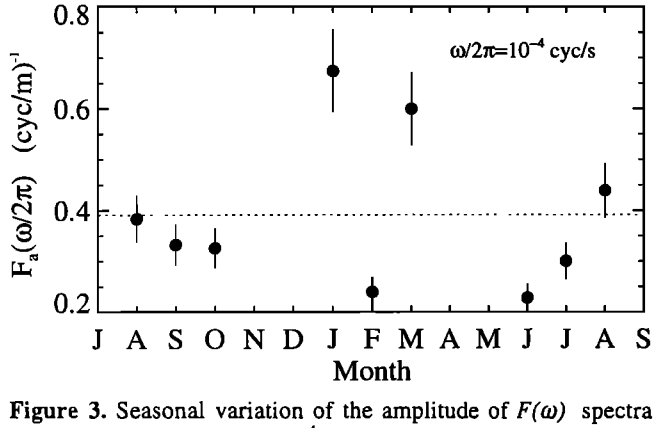

Figure 3. Seasonal variation of the amplitude of $F(\omega)$ spectra at the frequency of $\omega/2\pi = 10^{-4}$ (cycles/s). The dotted lines indicate the means of the slope and amplitude, respectively.

Table 2. Spectral Analysis Results for Three Altitude Regions

Measurement Site	Spectral Slope	Spectral Magnitude at $\omega/2\pi = 10^{-4}$(cycle/s)
Rayleigh lidar 25-40 km Kahalui, Maui	-1.2	0.2
Rayleigh lidar 45-75 km Logan, Utah	-1.5±0.3	0.4
Sodium lidar ~80-105 km Kahalui, Maui	-1.8	2.0

The slopes and the magnitudes of spectra for the upper stratosphere and the mesopause regions are taken from the plot presented by *Hostetler and Gardner* [1994].

mean. These high spectral magnitudes are associated with the low-frequency wave activity possibly produced by the planetary waves known to appear in the winter mesosphere [*Hauchecorne and Chanin*, 1993].

Even though there are numerous $F(\omega)$ spectra published for the mesopause region based on Na lidar observations, there are very few Rayleigh lidar $F(\omega)$ spectra published for the altitude ranges of the upper troposphere and the lower and middle mesosphere regions. One set of $F(\omega)$ spectral results for the upper stratosphere (25-40 km) is based upon a series of ground-based lidar observations at Kahalui, Maui during the ALOHA-90 campaign [*Hostetler and Gardner*, 1994]. Another set was presented as part of a comparison of Rayleigh lidar and stratosphere-troposphere radar observations at Aberystwyth by *Mitchell et al.* [1994]. Table 2 presents a comparison of the values of the spectral indices for the upper stratosphere $F(\omega)$ spectrum from Kahalui (20-45 km), the averaged spectrum from Utah lidar (45-70 km), and a spectrum based upon the mesopause region from the Na lidar measurement at Kahalui, Maui, during the ALOHA-90 campaign. From this table, it can be seen that at the temporal frequency of $\omega/2\pi = 10^{-4}$ (cycle/s), the spectral magnitude for the $F(\omega)$ spectra increases from the lower to the higher atmosphere regions, while the slope index appears to be getting steeper with height. It must be noted that the ALOHA results for the upper stratosphere and mesopause were from a single night set of observations. The Abserystwyth results obtained for altitudes between 5 and 50 km showed no consistent trend, although *Mitchell et al.* [1994] presented interesting evidence showing $F(m)$ spectral indices becoming steeper with a decrease of wind speed for altitudes in the range between 5 and 15 km.

Even though there has been no additional lidar data published for the upper troposphere, there are many sodium lidar observations for the mesopause region, and the results from those observations are consistent with the ALOHA-90 data cited here. It is reasonable to conclude that the magnitudes of the temporal spectra from the mesopause region are generally ~2 to 5 times higher than that for the lower mesosphere region (45-70 km).

5. Vertical Wavenumber Spectra of Relative Density Perturbations

$F(m)$ spectra based on r_a profiles were calculated using the Utah Rayleigh data, and these are presented in the monthly av-

eraged format in Figure 4. The noise level floor has been subtracted in these results. The spectral magnitude is plotted against wavenumber in the usual log-log scale format. Typically, the number of hours of lidar data used to determine these spectra ranged from ~10 hour (May 1994) to a maximum of ~80 hour (September 1994) with a total of ~448 hours over 12 months. The portion of the spectrum where the signal-to-noise ratio falls below 1 is not plotted. The smallest wavelengths that can be resolved in these spectra change from month to month depending on the signal quality. The scale for the right-hand ordinate is for the $F(m)$ spectra of the horizontal wind perturbation produced by applying the scale factor $(g/N)^2$ to the left-hand axis. Also shown for reference in these plots are the linear instability spectral modes of the m^{-3} power law predicted by LIT [*Dewan and Good*, 1986] corresponding to the limits of monochromatic wave activity (α=1/2, dashed line) and the broad band wave activity (α=1/20, dotted line).

For the 12 months of data studied, the spectral amplitudes for the wavelengths between ~2 and 12 km fall between these two lines. The measured spectra tend to be in better agreement with the spectral model for monochromatic gravity wave activity. With most spectra, the spectral magnitudes lie close to or are slightly smaller than the upper limit given by the linear instability theory. However, the spectral magnitude for the December 1994 observations is ~2 times this limit.

Generally speaking, each of the spectra is partitioned into two parts, a portion with a linear trend and a portion that transitions from the linear region to a region of constant spectral magnitude seen for λ of ~8 km or higher. The slope of the spectra for the linear portions is compatible with the theoretically predicted value of -3, which can be seen when the curves in this portion are compared with the reference model also plotted. There is no clear turning point between these two parts of the spectrum, and the wavenumber range of the linear region varies from month to month. The month-to-month behavior will be discussed further below.

The overall 12-month average $F(m)$ spectrum is presented in Figure 5. It shows a power index value of -2.3±0.1 with the error estimation of the calculated slope evaluated from the goodness of the linear fit. To determine the characteristic vertical wavenumber m_* quantitatively, an area-preserved spectrum for the overall 12-month averaged spectrum has been calculated and plotted in Figure 6. The curve peaks at $m_* = 8\times10^{-5}$ cycles/m, which corresponds to the characteristic vertical wavelength of 12.2 km.

The calculated overall $F(m)$ spectrum was compared with the spectral model derived from the scale-independent diffusive filtering theory by *Gardner* [1994], which used values of m_* and α, the slope of the linear portion of the measured $F(\omega)$ spectrum. The results of this comparison are displayed in Figure 7, which shows that the experimental spectrum generally follows the DFT theoretical prediction of -1.98 for the wavelength region from 2 to 12 km. For the vertical scales >12 km, for decreasing wavenumber, the model spectrum shows a decrease of spectral magnitude while the data still show a slight increase. We conclude from this comparison that the scale-independent DFT model appears to work well for the mesosphere region, although a definitive test would be a mesosphere measurement of $F(m)$ for vertical winds, as suggested by *Gardner* [1996].

A caveat to this conclusion is a matter raised by *Mitchell et al.* [1994] but also discussed by *Fritts and Van Zandt* [1987]. The issue is the Doppler shift of spectral energy to lower or higher wavenumbers that may result from the propagation of gravity waves through a background wind field. The direction of shift depends upon the direction of wave propagation relative to the background flow. Such shifts may have the effect of increasing or decreasing the $F(m)$ slope parameter p.

Eckermann [1995] presented an extended discussion of the possible influence of variations in the background wind field upon p for several regions of the atmosphere. Evidence summarized in this review of the observational literature strongly suggests that variability in the spectral shape of $F(m)$ can be a consequence of changes in the background wind field, especially for the region of the mesosphere (55-80 km) where during the winter there exists a reversal of the zonal wind with a region of large wind shear. This work also suggested another mechanism by which the background wind field may influence the $F(m)$ spectral shape. The new idea described by Eckermann is that a shear in the background wind speed with height may refract waves to smaller vertical wavenumbers rendering the spectral slope steeper.

Our results on the vertical wavenumber spectra for lower mesosphere data for both winter and summer seasons do show indications of variability. Examination of $F(m)$ spectra for summer months (June, July, and August 1995) shows these to exhibit considerably flatter spectra than those for the winter months (December, January, and February 1994/1995). Because tidal models predict higher eastward winds in the winter zonal jet when compared with the speeds of westward winds in the summer jet, our results suggest higher values for the slope parameter p for the winter when the zonal winds are larger. This behavior is just the opposite of that reported by *Mitchell et al.* [1994] for winds in the lower stratosphere. Because it is known that a large vertical shear exists in the winter mesosphere between 55 and 75 km [*Hagen*, 1996], our results are consistent with the prediction of Eckermann's [1995] refractive shifting mechanism of increased steepness with greater wind shear.

The question of whether these curvature effects are real requires a consideration of statistical errors. The error analysis presented in the appendix describes the determination of the error estimate for spectral magnitudes in the overall-averaged spectrum. The result is that the standard deviation is ~10% of the spectral magnitude at each point. For the monthly averaged spectrum, the reduction of the sampling time to a fraction of the ~450 hr of the overall average spectrum makes the individual error estimates for the standard deviation vary from ~30 to 70% (~50 and ~10 hours, respectively) at each wavenumber. Considering the number of points in each spectrum and the magnitudes of individual error estimates, the variations seen in the spectral shapes from one month to the next are believed to be real. We note that the reproducibility of the spectral shapes for the 2 months of August and September 1994, as compared with the spectral shapes of August and September 1995, provides confidence that these variations are not related to noise fluctuations. We conclude that these $F(m)$ spectral shapes do indicate a systematic seasonal trend in which the spectra become steeper in the transition from summer to winter. A similar behavior was reported by *Marsh et al.* [1991].

Thus the overall implication that underlies these results is that future $F(\omega)$ and $F(m)$ spectral measurements for the upper stratosphere and mesosphere regions should be accompanied by direct measurements of the background wind field so that

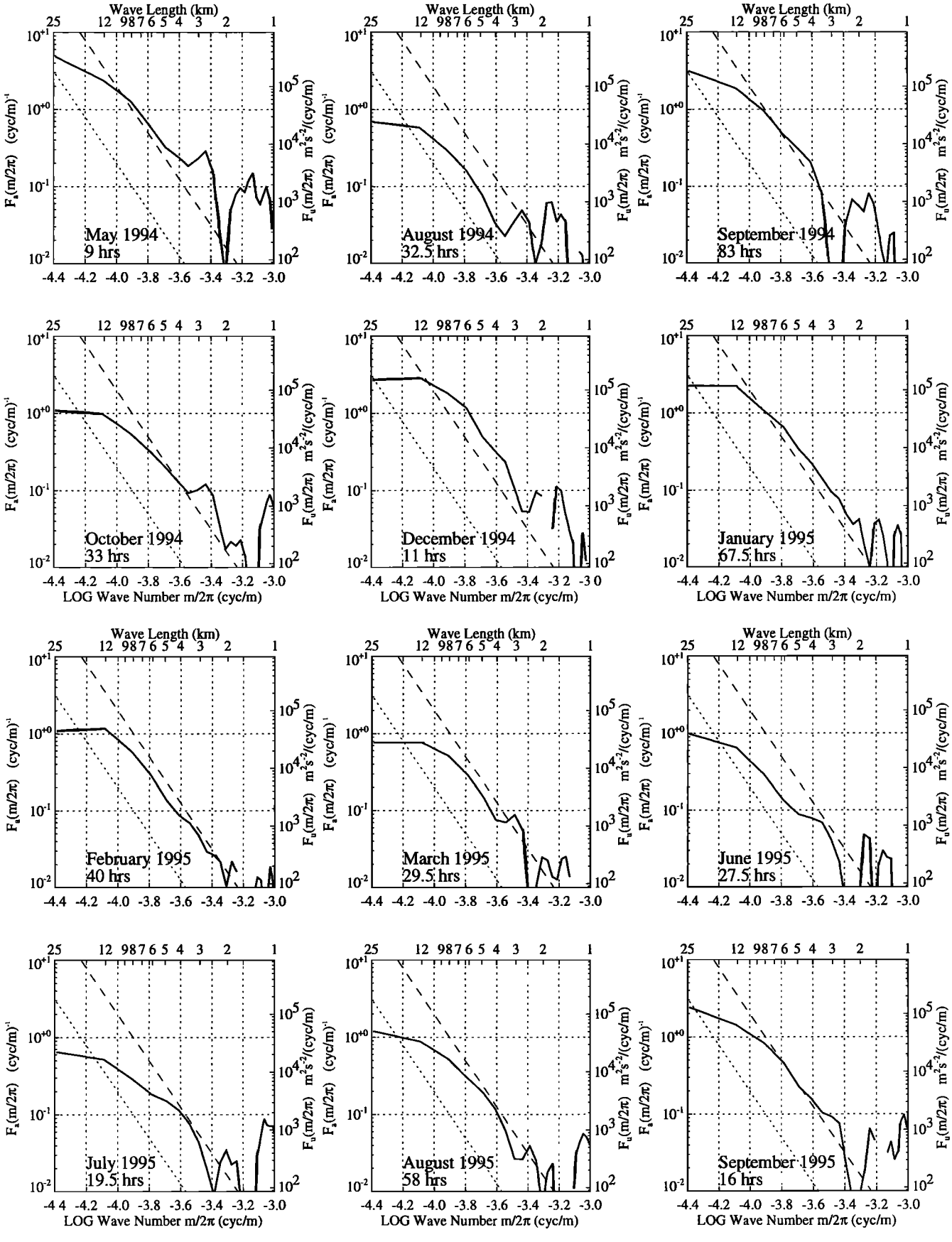

Figure 4. Monthly averaged vertical wavenumber spectra. The number of hours of observations is also indicated for each case plotted. The linear saturation model spectra for the case of monochromatic wave (dashed lines) and for the case of wave packet (dotted lines) are plotted for the altitude range between 45 and 70 km.

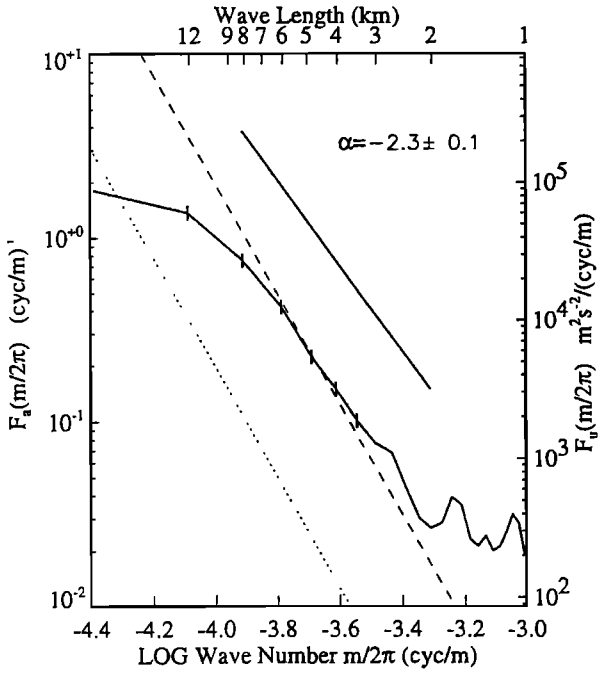

Figure 5. Overall *F(m)* spectrum.

Doppler-shifting effects can be assessed quantitatively. Such measurements are possible with a Doppler Rayleigh lidar, which is undergoing development in several Rayleigh lidar groups [*Chanin et al.*, 1989; *Tepley et al.*, 1993]. It should be possible to use this information to examine the relationship between the behavior of the background winds and the spectral slope parameter p, and this is an obvious direction for future work.

The question then arises as to the significance of the comparison of the overall *F(m)* spectrum with the SIDFT prediction

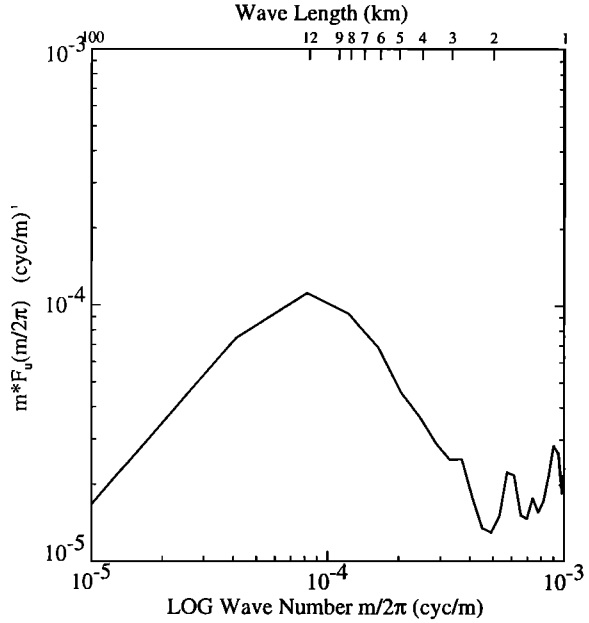

Figure 6. The area preserved *F(m)* spectrum obtained after averaging over all 12 months. The wavelength corresponding to the spectral maximum is 12.2 km.

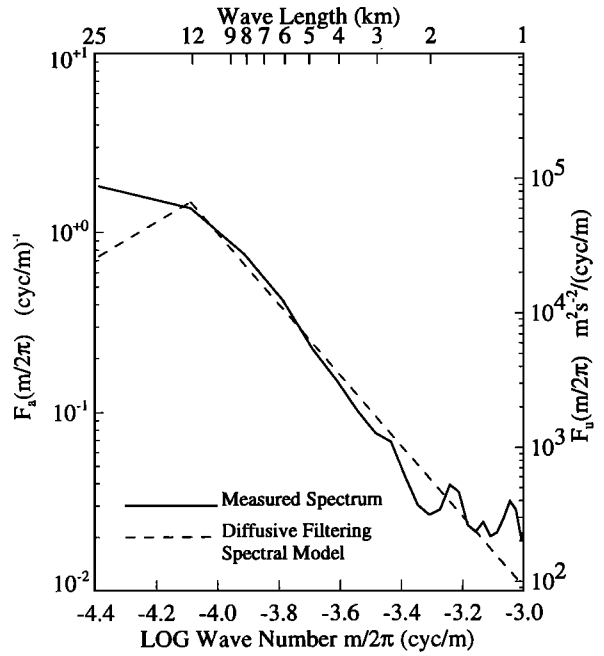

Figure 7. The comparison of the measured *F(m)* spectrum with the spectral model derived from the scale-independent diffusive filtering theory. The parameters p and m_* used to generate the model spectrum are inferred from the *F(ω)* spectrum. The *F(m)* spectrum is calculated from the Rayleigh data. Other parameters used to generate the model spectrum are: $s = 1$, $N = 2\pi/(5\text{min})$, $R_i \approx 1$, and $f = 2\pi/(18\text{hours})$.

that is presented in Figure 5. The appearance of the overall-averaged *F(m)* spectral shape presented in Figure 5 is similar to that seen in the monthly averaged spectrum for the equinoxes, when it is known that the background winds are weak. Thus it can be argued that the Doppler-shifting effects would be reduced by the averaging of measurements for all four seasons. Certainly, however, until the Doppler-shifting effects are understood more clearly, our conclusion that the DFT theory works well for the mesosphere region must remain tentative.

It was pointed out by *Smith et al.* [1987] that for the region of high vertical wavenumbers, where $m/m_* >> 1$, the characteristic vertical wavenumber may be computed from the relation

$$m_* \propto \left(m^3 F(m) / E\right)^{1/2} \tag{23}$$

where *F(m)* is the vertical wavenumber spectrum and E is the kinetic energy per unit mass. Within the scope of linear instability theory, *F(m)* does not change with height at a given wavenumber m, but E will change with height at a rate given by

$$E \propto e^{z/H_E} . \tag{24}$$

For mesospheric heights, H_E will vary from 14 to 21 km. Thus

$$m_* \propto e^{-z/2H_E} . \tag{25}$$

The decrease of m_* with increasing altitude has been observed by several experimental groups. Studies by *Sato and Woodman* [1982] and *Barat* [1983] suggested the dominant vertical wavelength of 1-2 km for the lower stratosphere. For comparison, the results of the characteristic wavelengths from

Table 3. Characteristic Wavenumbers Observed for Selected Mesospheric Height Ranges

	Observation range, km	$\lambda_m=2\pi/m_m$, km	References
XeF lidar, Japan	30-65	~10	*Shibata, et al.*[1986]
Rayleigh lidar, Illinois	35-50	~7-10	*Gardner et al.*[1989]
Rayleigh lidar, France	30-70	~8-15	*Chanin and Hauchecorne*[1981]
Rayleigh lidar, France	55-70	~6	*Wilson et al.* [1991]
Rayleigh lidar, Utah	45-70	~12	This study
Radar observation	60-110	~10-15	*Meek et al* [1985] *Manson and Meek* [1988]
Sodium lidar, Arecibo	83-102	~14.3	*Senft et al.* [1993]

other lidar observations for the mesosphere region have been tabulated in Table 3. It can be seen that the characteristic vertical wavelength derived from the Utah data is in agreement with the other lidar and radar observations of the mesosphere region.

Our work along with other Rayleigh lidar results listed in Table 3 found that the dominant vertical wavelength is ~6-12 km for the region from the upper stratosphere to the middle mesosphere. For the mesopause, the sodium lidar results suggest a dominant vertical wavelength of about 14 km. While the results do not fit the theoretical prediction in (11), nevertheless, they do demonstrate a decrease of m_m with increasing altitude.

The seasonal variation of the spectral amplitude of the $F(m)$ spectra was also studied. The observed spectral magnitudes at the vertical wavenumber $m/2\pi = 10^{-1}$ (1/10 km) for the examined period are plotted in Figure 8. This choice of wavenumber was based upon the fact that the ratio of signal to noise at higher wavenumbers was considerably smaller due to the high magnitude of the noise floor. *Senft and Gardner* [1991] presented similar results for three wavenumbers (2, 4, and 8 km scales) deduced from the analysis of sodium lidar observations and found the data at 2 km wavelength to exhibt the least variability.

The plot shows an annual variation of the spectral amplitude with a peak in winter months and a valley in summer months. The thick curve is the 6th-order polynomial fit to the data. The mean spectral magnitude of 4.1×10^{-5} m^2s^2/(cycles/m) is indicated by the dashed horizontal line. The winter peak value is about 1.5 times higher than the mean and 3 times higher than the summer spectral magnitude. This variation agrees with the annual variation seen in the climatological study of the density and temperature perturbations that showed strong low frequency wave activity in the mesospheric region during the winter over the Rocky Mountains. This result is also in good agreement with the results reported by *Wilson et. al.* [1991] for the series of Rayleigh lidar observations in Verrieres Le Buission, France. Their data between 1986 and 1989 covered the range of altitudes from 30 to 70 km. The annual variations of the gravity wave magnitudes at middle and high latitudes have been reported by other groups by using different instrumentation [*Hirota*, 1984; *Theon et al.*, 1976, *Smith et al.*, 1968].

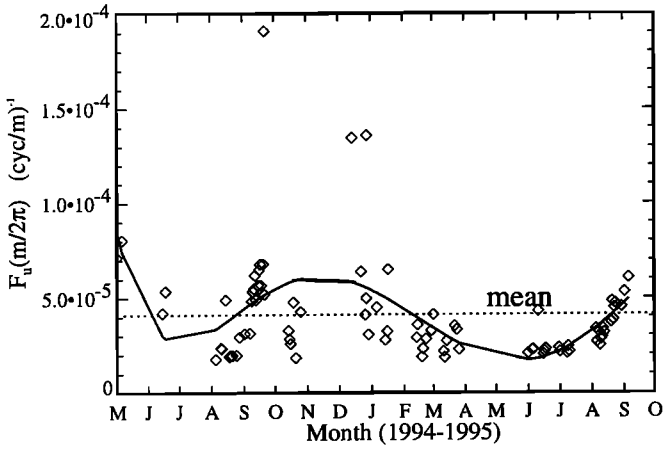

Figure 8. The seasonal variation of the $F_u(m)$ spectral amplitude at the vertical wavenumber $m/2\pi = 10^{-4}$ m.

It is interesting to note how the climatology of the seasonal variation of the vertical wavenumber magnitudes exhibited by the Rayleigh lidar results contrasts with the results found for the sodium lidar observations reported by *Collins et al.* [1996]. This paper analyzed the seasonal variation of the m-spectral magnitude values deduced from sodium lidar observations and found a semiannual variation with maximum values noted for summer and winter and minimal values found for equinoctial periods. We note that the Rayleigh results presented here would be more subject to masking generated by planetary wave activity. Furthermore, it is reasonable that the mesopause region of the sodium layer would experience greater gravity wave activity in the summer than the upper mesosphere region sampled by the Utah Rayleigh lidar. In this season, the waves are generated at the source with small amplitudes and can propagate to higher altitudes before breaking.

6. Conclusions

In this paper, the technique of spectral analysis featuring the method of pre-whitening and post-darkening [*Dewan et al.*, 1988] has been applied to the analysis of the Utah lidar mesosphere density perturbation data. Both $F(\omega)$ and $F(m)$ spectra have been calculated for the mesosphere height range of 45-70 km. The results from this spectral analysis have been compared with two spectral models based on the linear saturation theory and the scale-independent diffusive filtering theory. The comparison of the experimental $F(m)$ spectrum to the DFT-predicted $F(m)$ spectrum based upon the measured slope parameter p of the $F(m)$ spectrum showed there was good agreement between the two curves. However, this comparison

cannot be considered definitive without knowledge of possible Doppler-shifting effects.

The $F(\omega)$ spectrum when averaged over the total of 9 months of data revealed a spectral slope of -1.49±0.03. This result is in reasonable agreement with the results from other observations and with the LIT prediction of -5/3 (-1.67). These spectra show a slight degree of month-to-month variation in values of both the spectral slope and magnitude, but no significant seasonal variation was found that might be a result of seasonal variation in the wind field as suggested by *Mitchell et al.* [1994]. The implication is that for an observatory located in a region of active atmospheric dynamics, an accurate determination of the slope parameter α will likely require averaging over a larger number of lidar data samples, perhaps in excess of 100 hours total.

Comparison of our results with other published $F(\omega)$ spectra for different height ranges showed a tendency for the spectral magnitude to increase with height. While the experimental $F(m)$ spectrum shows a flatter slope compared with the model spectrum based on the linear instability theory, the experimental result agreed well with the DFT model spectrum in both spectral slope and magnitude. However, this conclusion has to be qualified by the concern regarding the extent that the $F(\omega)$ and $F(m)$ spectra may have been contaminated by Doppler-shifting effects. Examination of the monthly averaged $F(m)$ spectra showed indications of a systematic shift of the slope parameter p with season that is consistent with the picture of a background wind field that reverses between winter and summer. The increased steepness of the slope for winter observations is consistent with the known increase of winter stratospheric wind speeds.

The overall-averaged $F(m)$ spectra has a linear portion in the spectrum with a spectral slope of -2.3 ±0.1. This spectral slope is flatter than the value of -3 predicted by the linear instability theory. The spectral magnitude lies close to the spectral magnitude limit for monochromatic wave activity, even though a broadband spectrum of gravity wave activity was found for the temperature and density perturbation profiles.

The analysis showed a characteristic wavelength of ~12 km for the mesospheric altitude range (45-70 km). Comparison of this value with values of the characteristic wave length found for observations in the stratosphere and mesopause regions showed qualitatively an increase of λ_z with height.

The seasonal variation of the $F(m)$ spectral magnitudes is obvious with maximum values found for winter measurements. This enhancement of the spectral magnitude may be a result of the low frequency wave activity evident in the winter temperature perturbation profiles.

Appendix: Standard Deviation of Calculated Spectra

The analysis of the statistical errors involves the consideration of both the direct spectral estimator and the smoothing window. For a stationary process $\{X_t\}$ with a spectral density function $S(f)$, the periodogram of $\{X_t\}$, S^p, satisfies

$$S^p(f) \Rightarrow S(f)\chi_2^2/2 \quad \text{for } 0 < f < f(N) \tag{A1}$$

$$\text{var}\left\{S^p(f)\right\} \Rightarrow S^2(f), \quad \text{for } 0 < f < f(N), \tag{A2}$$

where $\Rightarrow$ stands for "equal in distribution", $f(N)$ is the Nyquist frequency, and χ_2^2 is the chi-square distribution with 2 degrees of freedom. For a process in which the autocovariance function is summable and the data window function is reasonable in form, the distribution of the magnitude of the direct spectral estimation $S^d(f)$ is the same as that for the periodogram. That is,

$$S^d(f) \Rightarrow S(f)\chi_2^2/2 \quad \text{for } 0 < f < f(N) \tag{A3}$$

and

$$\text{var}\left\{S^d(f)\right\} \Rightarrow S^2(f) \quad \text{for } 0 < f < f(N) \tag{A4}$$

Taking the estimation value on both sides of (A3), we find

$$E\{S^d(f)\} = E\{S(f)\chi_2^2/2\} = S(f). \tag{A5}$$

This indicates that we can use the average value of $S^p(f)$ to approximate $S(f)$.

We use a smoothing window to decrease the variance. For the Bartlett window the asymptotic variance is given by

$$\text{var}\{S^{lw}(f)\} = \frac{0.67mC_h(S^d(f))}{N} = \frac{0.67mC_hS^2(f)}{N} \tag{A6}$$

where $S^{lw}(f)$ is the spectral magnitude from a lag window spectral estimator and m is the lag window parameter which is 1/5 N for most cases of the data analyzed in our paper. C_h is the variance inflation factor, which can be calculated for large N by the formula given by *Percival and Walden* [1993]

$$C_h = N\sum_{t=1}^{N} h_t^4 \tag{A7}$$

where h_t is the rectangular taper window function. Evaluation leads to C_h=1. Thus the variance for each individual lag window smoothed direct spectral estimation is

$$\text{var}\{S^{lw}(f)\} = 0.134S^2(f). \tag{A8}$$

According to the Central Limit Theorem, the sample distribution of the mean is very close to the normal distribution. Hence, for the averaged spectrum,

$$\text{var}\{\overline{S^{lw}}(f)\} = (E\{S^{lw}(f)\})^2/n \tag{A9}$$

In our case n=16, and therefore

$$\text{var}\{\overline{S^{lw}}(f)\} = 0.008S^2(f). \tag{A10}$$

The corresponding standard deviation for the averaged spectrum is therefore the square root of the variance or ~$0.09S(f)$.

Acknowledgments. The encouragement provided by Chet Gardner and his critique of an early draft of this paper are very much appreciated. This research was supported by grants from the CEDAR NSF Aeronomy program at the National Science Foundation to Clemson University and to Utah State University.

References

Barat, J , The fine structure of the stratosphere flow revealed by differential sounding, *J. Geophys. Res., 88*, 5219-5228, 1983.

Beatty, T. J., C A. Hostetler, and C. S. Gardner, Lidar observations of gravity waves and their spectra near the mesopause and stratopause at Arecibo, *J. Atmos. Sci., 49*, 477-496, 1992.

Chanin, M. L., and A. Hauchcorne, Lidar observation of gravity wave and tidal waves in the stratosphere and mesosphere, *J Geophys. Res., 86*, 9715-9721, 1981.

Chanin, M.L., A. Garnier, A. Hauchecorne, and J. Porteneuve, A doppler lidar for measuring winds in the middle atmosphere, *Geophys. Res. Lett., 16*, 1273-1276, 1989.

Collins, R. L., X. Tao, and C.S. Gardner, Lidar observations of gravity wave activity in the upper mesosphere over Urbana, Illinois: Lidar observations and analysis of gravity wave propagation models, *J. Atmos. Terr. Phys., 58*, 1905-1926, 1996.

Dewan, E. M., Similitude modeling of internal gravity wave spectra, *Geophys. Res. Lett., 18*, 1473-1476, 1991.

Dewan, E. M., The saturated-cascade model for atmospheric gravity wave spectra, and the wavelength-period (W-P) relations, *Geophys. Res. Lett., 21*, 817-820,1994.

Dewan, E. M., The saturated-cascade similitude theory of gravity wave spectra, J. Geophys. Res., in press, 1997.

Dewan, E. M., and R. E. Good, Saturation and the "universal" spectrum vertical profiles of horizontal scalar winds in the atmosphere, *J. Geophys. Res, 91*, 2742-2748, 1986.

Dewan, E.M., N. Grossbard, R. E. Good, and J. Brown, Power spectral density of zonal and meridional winds in the stratosphere, *Phys. Scr., 37*, 154-157, 1988.

Eckermann, S. D., Effect of background winds on vertical wavenumber spectra of atmospheric gravity waves, *J. Geophys. Res., 100*, 14,097-14,112, 1995.

Fritts, D.C., and T.E. VanZandt, Effects of Doppler shifting on the frequency spectra of atmospheric gravity waves, *J. Geophys. Res., 92*, 9723-9732, 1987

Gardner, C S., Diffusive filtering theory of gravity wave spectra in the atmosphere, *J. Geophys. Res., 99*, 20,601-20,622, 1994.

Gardner, C. S., Gravity wave models for the horizontal wavenumber spectra of atmospheric velocity and density fluctuations, *J. Geophys. Res., 98*, 1035-1049, 20, 1993.

Gardner C. S., M. S. Miller, and C.H. Liu, Rayleigh lidar observations of gravity wave activity in the upper stratosphere at Urbana, Illinois, *J. Atmos. Sci., 46*, 1838-1854, 1989.

Gardner, C. S., Scale-independent diffusive filtering theory of gravity wave spectra in the atmosphere, The upper mesosphere and lower thermosphere: A review of experiments and theory, *J. Atmos. Terr. Phys., 58*, 1575-1589,1996.

Gardner, C. S., Testing theory of atmospheric gravity wave saturation and dissipation, *J. Atmos. Terr. Phys., 58*, 1575-1589, 1996.

Garrett, C , and W. Munk, Space-time scales of internal waves: A progress report, *J. Geophys. Res., 80*, 291-297, 1975.

Hagan, M. E., Comparative effects of migrating solar sources on tidal signatures in the middle and upper atmosphere, J.Geophys. Res., 21, 213-21,222, 1996.

Hauchecorne, A., and M. L. Chanin, Midlatitude lidar observations of planetary waves in the middle atmosphere during the winter of 1981-1982, *J. Geophys. Res., 88*, 3843-3849, 1983.

Hines, C. O., Internal atmospneric gravity waves at ionospheric heights, *The Upper Atmosphere in Motion*, 248-298, 1960.

Hines, C. O., The saturation of gravity waves in the middle atmosphere, II, Development of Dopploer-spread theory, *J. Atmos. Sci.. 48*, 1360-1379, 1991.

Hirota, I., Climatology of gravity waves in the atmosphere, *J. Atmos. Terr. Phys., 46*, 767-773, 1984.

Hostetler, C. A., and C. S. Gardner, Observation of horizontal and vertical wavenumber spectra of gravity wave motions in the stratosphere and mesosphere over the mid Pacific, *J. Geophys. Res., 99*, 1283-1302, 1994.

Manson, A. H., and C. E. Meek, Gravity wave propagation characteristics (6-120 km) as determined by the Saskatoon MF radar (Gravnet) system: 1983-85 at 52 N, 107 W, *J. Atmos. Sci., 45*, 932-946, 1988.

Marsh, A. K., N. J. Mitchell, and L. Thomas, Lidar study of stratospheric gravity-wave spectra, *Planet. Space Sci, 39*, 1542-1548, 1991.

Meek, C. E., I. M. Reid and A. H. Manson, Observation of mesospheric wind velocities. I: Gravity wave horizontal scales and phase velocities from spaced wind observations, *Radio Sci., 20*, 1363-1383, 1985.

Mitchell, N J , L. Thomas, and A. P K. Marsh, Lidar studies of stratospheric gravity waves: A comparison of analysis techniques, *Ann. Geophys., 8*, 705-712, 1990.

Mitchell, N.J., L. Thomas and I.T. Prichard, Gravity waves in the stratosphere and troposphere observed by lidar and MST radar, *J. Atmos. Terr. Phys., 56*, 939-947,1994.

Percival, D. B. and A. T. Walden A. T., *Spectral Analysis for Physical Applications*, Cambridge Univ. Press, New York, 1993.

Sato, T., and R. F. Woodman, Fine altitude resolution radar observations of upper-tropospheric and lower-stratospheric winds and waves, *J. Atmos. Sci., 39*, 2539-2545, 1982.

Senft, D. C., and C. S. Gardner, Seasonal variability of gravity wave activity and spectra in the mesopause region at Urbana, *J. Geophys. Res., 96*, 17,229-17,264, 1991.

Senft, D. C., C.A. Hostetler, and C.S. Gardner, Characteristics of gravity wave activity and spectra in the upper stratosphere and upper mesosphere at Arecibo during early April 1989, *J. Atmos. Terr. Phys., 55*, 425-439,1993.

Shibata, T., M. Kobuchi, and M. Meada, Density flucturation in the middle atmosphere over Fukuoka observed by a XeF Rayleigh lidar, *Geophys. Res. Lett., 13*. 1121-1124, 1986.

Smith, W. S., L. B. Katchen, and J. S. Theon, Grenade experiments in a program of synoptic meteorological measurements, *Meteorol. Monogr. 9*, 170-175, 1968.

Smith, W. S., D. C. Fritts, and T. E. VanZandt, Evidence for a saturated spectrum of atmospheric gravity waves, *J. Atmos. Sci., 44*, 1404-1410, 1987.

Tepley, C. A., S. I. Sargoytchev, and R. Rojas, The Doppler Rayleigh lidar system at Arecibo, *IEEE Trans. Geosci. Remote Sens., 31*, 36-47, 1993.

Theon, J. S., W. Nordberg, and L. B. Hatchen, *J. Atmos. Sci., 24*, 428-438, 1976.

Van Zandt, T. E., A universal spectrum of buoyancy waves in the atmosphere, *Geophys. Res. Lett., 9*, 575-578, 1982.

Weinstock, J., Saturated and unsaturated spectra of gravity waves and scale-dependent diffusion, *J. Atmos. Sci. 47*, 2211-2255, 1990.

Whiteway, J. A., and A. L. Carswell, Rayleigh lidar observation of thermal structure and gravity wave activity in the high Arctic during a stratospheric warming, *J. Atmos. Sci., 51*, 3122-3136, 1994.

Wilson, R., M. L. Chanin, and A. Hauchecorne, Gravity waves in the middle atmosphere observed by Rayleigh lidar, 1., Case studies, *J. Geophys. Res., 96*, 5153-5167, 1991.

S. Collins, Arecibo Observatory, P.O. Box 995, Arecibo, PR 00613

X. Gao, Electro-optic Systems Laboratory, University of Illinois, Urbana, IL 61801

J. W. Meriwether, Department of Physics and Astronomy, Clemson University, Clemson, SC 29634-1911. (e-mail: john.meriwether @ces.clemson.edu)

V. B. Wickwar, and T D. Wilkerson, Center of Atmospheric and Space Physics, Utah State University, Logan, UT 84322

(Received February 25, 1997; revised August 4, 1997; accepted September 2, 1997.)